Available online at www.sciencedirect.com
ScienceDirect
International Journal of Heat and Fluid Flow 28 (2007) 708–719
International Journal of HEAT AND FLUID FLOW
www.elsevier.com/locate/ijhff

# Flow field analysis of a turbulent slot air jet impinging on a moving flat surface

J. Senter, C. Solliec *

*GEPEA UMR-CNRS 6144, Ecole des Mines de Nantes, Département Systèmes Energétiques et Environnement, 4, rue Alfred Kastler, B.P. 20722, 44307 Nantes, France*

Received 6 April 2006; received in revised form 14 July 2006; accepted 25 August 2006
Available online 17 October 2006

**Abstract**

The flow field topology of a confined turbulent slot air jet impinging normally on a moving flat surface has been investigated experimentally by using particle image velocimetry (PIV). Experiments were conducted for a nozzle-to-plate spacing of eight slot nozzle widths, at three Reynolds numbers ($Re = 5300$, 8000 and 10,600) and four surface-to-jet velocity ratios i.e. 0, 0.25, 0.5 and 1. The measurements of the mean velocities and turbulent quantities are presented in the following main characteristic regions of the jet: the potential core, the intermediate zone and the impinging zone. It appears that the flow field patterns at a given surface-to-jet velocity ratio are independent of the jet Reynolds number in the range of 5300–10,600. A slight modification of the flow field is observed for a surface-to-jet velocity ratio of 0.25 whereas at higher ratios of 0.5 and 1, the flow field is significantly affected.


*Keywords:* Impinging jet; Moving surface; PIV; Turbulence

## 1. Introduction

Impinging jets have received considerable research attention because of the high convective heat transfer that occurs in the impingement region (Korger and Krizek, 1966; Antonia, 1983; Viskanta, 1993; Sakakibara et al., 1997; Haneda et al., 1998; Narayanan et al., 2004). Industrial applications include tempering and shaping glass, drying textiles and paper, cooling turbine blades and electronic equipment, annealing metal and plastic sheets and some processes in the food industry. Thus, the jet flow issuing from a nozzle is often directed perpendicular to a moving impingement surface (Fig. 1). Some numerical studies have reported the strong effects of the impingement surface motion on the fluid flow (Zumbrunnen, 1991; Chattopadhyay and Saha, 2003). The flow field can be significantly affected since the impingement surface velocity can exceed the jet velocity in some applications such as the hot-rolling process. Indeed, at the impingement, the jet flow is divided into two wall jets. The wall jets behaviour will consequently be completely different given that the wall jet flow moves in the same or in the opposite direction to the moving surface. As a result, the strongly modified flow field will influence the convective heat transfer. As reported by Schlünder et al. (1970) and later by Martin (1977), the heat and mass transfer in impinging flow depends on the Reynolds number, the Prandtl number of the fluid, nozzle geometry and nozzle-to-plate spacing. Gardon and Akfirat (1965, 1966) also noticed the effect of turbulence on the local heat and mass transfer. They reported that, for a slot air jet, the absolute magnitude of the velocity fluctuations reaches a maximum in the neighbourhood of a nozzle-to-plate spacing equals to eight slot nozzle widths. This maximum occurs simultaneously with the maximum of the heat transfer coefficient at the stagnation point. It is also important to point out the role of the confinement of the jet on the flow field (Fitzgerald and Garimella, 1998). Indeed, the heat transfer distribution along the impingement surface is generally characterised by a single peak located at the

* Corresponding author. Tel.: +33 2 5185 8265; fax: +33 2 5185 8299.
*E-mail address:* camille.solliec@emn.fr (C. Solliec).

0142-727X/$ - see front matter © 2006 Elsevier Inc. All rights reserved.
doi:10.1016/j.ijheatfluidflow.2006.08.002

**Nomenclature**

| | |
|---|---|
| $e$ | slot nozzle width |
| $h$ | heat transfer coefficient |
| $H$ | impingement distance |
| $k$ | turbulent kinetic energy |
| $k'$ | two-component turbulent kinetic energy, $(u_{rms}^2 + v_{rms}^2)$ |
| $I_U$ | turbulence intensity of the fluctuating component of velocity in the $x$-direction |
| $I_V$ | turbulence intensity of the fluctuating component of velocity in the $y$-direction |
| $L_C$ | potential core length |
| $l$ | channel width |
| $Nu$ | Nusselt number, $he/\lambda$ |
| $Re$ | Reynolds number, $U_J e/\nu$ |
| $R_{SJ}$ | surface-to-jet velocity ratio, $V_S/U_J$ |
| $U$ | mean velocity in the $x$-direction |
| $U_J$ | jet centerline mean velocity at nozzle exit |
| $u_{rms}$ | rms of the fluctuating component of velocity in the $x$-direction |
| $V$ | mean velocity in the $y$-direction |
| $v_{rms}$ | rms of the fluctuating component of velocity in the $y$-direction |
| $V_S$ | mean velocity of impingement surface in the $y$-direction |
| $(U^2 + V^2)^{1/2}$ | mean velocity magnitude |
| $\langle u'v' \rangle$ | mean Reynolds shear stress |
| $x$, $y$ | coordinates |

*Greek symbols*

| | |
|---|---|
| $\varepsilon$ | turbulent dissipation rate |
| $\lambda$ | thermal conductivity of air |
| $\nu$ | kinematic viscosity of air |
| $\rho$ | air density |

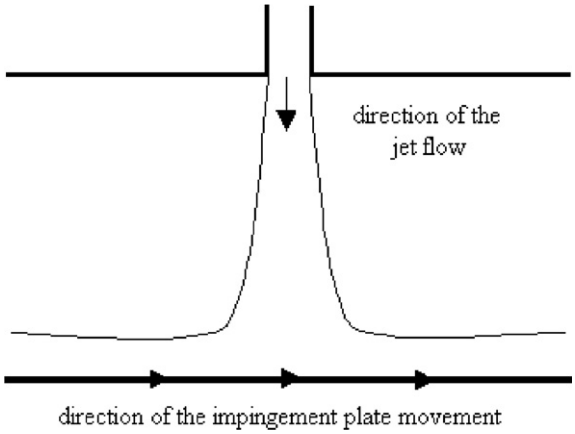


Fig. 1. Sketch showing the impingement plate movement relative to the jet flow direction.

stagnation point. However, at small nozzle-to-plate spacings, secondary peaks appear in the heat transfer distribution. They suggested that these peaks, generally understood to result from a transition to turbulence in the wall jet boundary layer, might also be due to the recirculation patterns found for the confined jet.

Among the very few experimental studies involving jets impinging on a moving flat surface, the work of Subba Raju and Schlünder (1977) concerning a moving flat surface impinged by a turbulent slot air jet can be mentioned. A mean heat transfer coefficient was calculated over the length of the impingement surface for different nozzle-to-plate spacings, several Reynolds numbers and a surface velocity $V_S$ between 0.15 m/s and 5.5 m/s. However, a lack of information about the local heat transfer and the flow field prevents an understanding of the physical phenomenon. Van Heiningen et al. (1977) performed an experimental study of a turbulent slot air jet impinging on a large rotating drum. The tangential velocity of the moving surface was less than 2% of the jet velocity. Under these conditions and comparing their results with the available data for a turbulent slot jet impinging on a stationary surface, they concluded that, for low surface-to-jet velocity ratios, the wall motion seemed to be negligible in the local heat transfer.

The aim of this paper is to investigate the role of surface motion in the development of a turbulent slot air jet impinging on a moving flat and smooth surface. The relative moderate Reynolds numbers considered in this study have been chosen to enable a first comparison with different numerical simulations where the roughness is not taken into account. It also seems important to have first an accurate description of this complex flow field to enable validation of the local heat transfer in future experimental and numerical studies. In addition, future research could considered the effects of surface roughness of the moving surface on the flow field and on the local heat transfer. Indeed, Beitelmal et al. (2000) investigated experimentally the effects of surface roughness on the average heat transfer characteristics of a circular air jet impinging on a stationary surface. The roughness took the form of a circular array of protrusions of 0.5 mm base and 0.5 mm height. They showed an increased of up to 6% of the average Nusselt number due to surface roughness. Finally, Chakroun et al. (1998) also mentioned the average Nusselt number increase of a stationary surface impinged by a circular air jet due to the effects of surface roughness. In that experimental study, the roughness was composed of 1 mm cubes and was found to affect significantly both the mean velocity and the turbulence intensity of the flow.

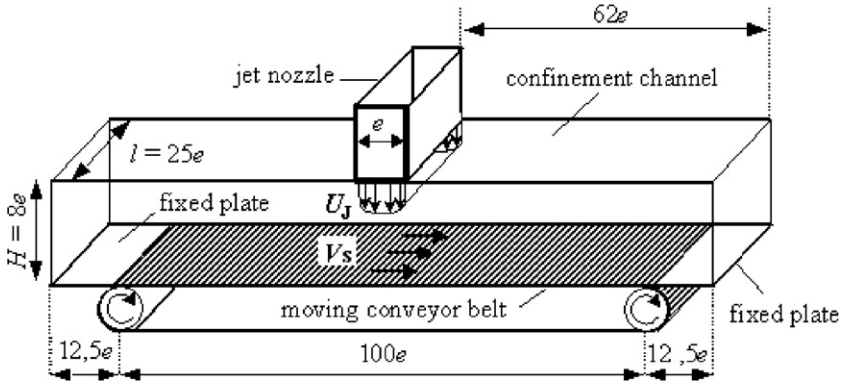


Fig. 2. Scheme of the experimental set-up.

## 2. Experiments

### 2.1. Experimental set-up and configuration cases

The apparatus used for the present investigation is depicted in Fig. 2. The air jet, blown at 20 °C, is generated by a centrifugal ventilator before passing through a diverging nozzle and a converging nozzle with a contraction ratio of 6.25. The slot nozzle width $e$ is 20 mm and the nozzle-to-plate spacing $H$ is $8e$. This distance is selected because it is known to generate the maximum heat transfer at the stagnation point (Metzger, 1962; Gardon and Akfirat, 1965). More recently, Gori and Bossi (2003) found the optimal slot height in the jet cooling of a circular cylinder to be $8e$. Then, the jet blows into a confinement tunnel from top to bottom. The width of the tunnel is 500 mm and its length is 2500 mm.

The nozzle aspect ratio $l/e$ is higher than 20, which enables the flow field to be considered two-dimensional, at least for the mean time properties (Rajaratnam, 1976; Awbi, 1991). The transversal distribution of the velocity at the nozzle exit $U_J$ fits well with a seventh power law profile. The nozzle exit turbulence intensity of component $U$ is about 9% (from PIV measurements). The three Reynolds numbers studied are 5300, 8000 and 10,600. They are based on the centerline velocity at the nozzle exit $U_J$ and the slot nozzle width $e$. The jet, located at the middle of the confinement tunnel, impinges on the moving surface perpendicularly.

The moving surface is an endless rubber belt, driven on two rollers, one of which is connected to a variable rotating speed motor. The strip stretched between the two rollers and slipped onto a fixed flat plate provides a continuous surface velocity controlled by a tachometer. Two plates are fixed at the ends of the conveyor belt to ensure no entry of fluid and thus to fulfill non-perturbing conditions at the exit of the wind tunnel. The maximum surface velocity $V_S$ reached is 8 m/s. The different cases studied are summarized in Table 1.

Table 1
Experimental cases

| Case | $V_S$ (m/s) | $U_J$ (m/s) | $Re$ | $R_{SJ}$ |
|---|---|---|---|---|
| 1 | 0, 1, 2, 4 | 4 | 5300 | 0, 0.25, 0.5, 1 |
| 2 | 0, 1.5, 3, 6 | 6 | 8000 | 0, 0.25, 0.5, 1 |
| 3 | 0, 2, 4, 8 | 8 | 10,600 | 0, 0.25, 0.5, 1 |

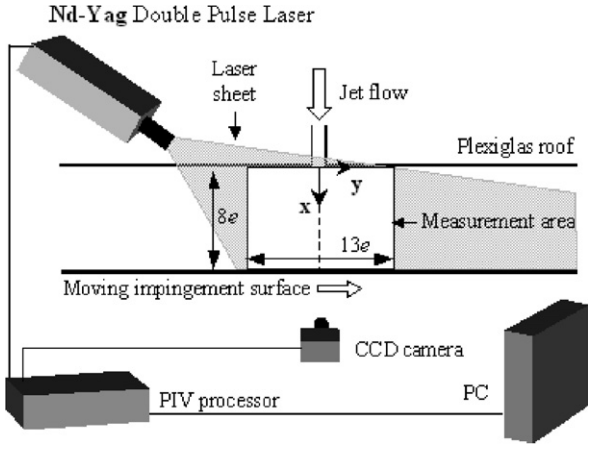


Fig. 3. Sketch showing the PIV data plane and the PIV system arrangement.

### 2.2. Particle image velocimetry

Fig. 3 shows the PIV system arrangement for the velocity measurements. For this purpose, the wind tunnel is made of Plexiglas to enable PIV velocity measurements in the $(x, y)$-plane. The origin of the $(x, y)$-coordinate system is at the intersection of the centerline of the jet and the top plates of the confinement tunnel. The $x$-axis is measured along this centerline and is assumed to be positive in the downward direction. The $y$-axis is measured along the top plates of the confinement wall. The measurement area is defined by $0 < x/e < 8$ and $-6.5 < y/e < 6.5$.

The impingement flow is investigated using a PIV system manufactured by Dantec Dynamics. The system includes a double-pulsed Nd-Yag laser ($2 \times 120$ mJ at 15 Hz and 532 nm). The laser is adjusted to produce a 1 mm thick sheet that illuminates the flow in the measurement area.

Seeding is obtained using an oil smoke generator. A high sensitivity double frame CCD camera with a

Table 2
Characteristics of the PIV measurements

| | |
|---|---|
| Focal length lens (mm) | 28 |
| Numerical aperture | 2.8 |
| Field of view (mm$^2$) | $202.7 \times 273.5$ |
| Interrogation area size (pixels$^2$/mm$^2$) | $32 \times 32/5.47 \times 5.47$ |
| Interrogation area overlap (%) | 50 |
| Reynolds number | 5300, 8000, 10,600 |
| Pulse delay (μs) | 200, 170, 130 |
| Dynamic velocity range (m/s) | 0.013:6.8, 0.016:8.0, 0.021:10.5 |
| Acquisition frequency of snapshots (Hz) | 15 |
| Number of snapshots | 700 |
| Maximum standard error for the first and second moments (%) | 2.8 and 7.4 |

resolution of $1186 \times 1600$ pixels$^2$ records the images of the seeding particles in the laser sheet. The PIV processor synchronizes the laser with the camera.

Table 2 presents the recording parameters of the PIV system for the three Reynolds numbers. Every 67 ms, a pair of images is recorded and the two images of each pair are separated by a pulse delay of varying duration. These pairs are then cross-correlated, which gives the seeding particle displacement between the two images and finally the instantaneous velocity field of the flow (Raffel et al., 1998). Each image is split into interrogation areas of $32 \times 32$ pixels$^2$, which leads to a map of $59 \times 98$ vectors$^2$. The percentage of spurious vectors rejected is less than 3% for a signal-to-noise ratio of 1.2. Moreover, the nearest vectors to the impingement surface ($x/e = 7.86$) should be interpreted carefully since the blooming generated by the laser sheet on the impingement surface can significantly bias their mean value. The maximum theoretical standard error (Bruun, 1995) has been estimated at 2.8% and 7.4%, respectively, for the first and second moments, to the entire region under investigation.

## 3. Results and discussion

The topologies of the flow field for the same surface-to-jet velocity ratio at different Reynolds numbers (5300, 8000, 10,600) are almost similar and will be studied first. Then, to clarify the analysis, the mean flow patterns, the mean velocities and the turbulent quantities will be examined in details only in the case of $Re = 10{,}600$.

### 3.1. Effect of the Reynolds number on the mean flow field

The experiments were conducted for a turbulent slot air jet at three Reynolds numbers of 5300, 8000 and 10,600 impinging on a surface animated by a velocity ratio $R_{SJ}$ of 0, 0.25, 0.5 and 1. This part of the study is carried out to investigate the influence of the jet Reynolds number on the mean flow field for a given surface-to-jet velocity ratio.

The distributions of the mean vertical velocity and the vertical turbulence intensity along the centerline are depicted in Fig. 4 for the three Reynolds numbers studied and the velocity ratio of 0, 0.5 and 1. These quantities represented along the centerline, and often used to characterize the jet impinging on a stationary surface, are interesting to compare with those of a jet impinging on a moving surface. Given that the profiles of these quantities for $R_{SJ} = 0.25$ are very similar to that for $R_{SJ} = 0$, they are not represented here to ensure a good readability. This similarity demonstrates the slight influence of the surface boundary layer on jet development and thus, the predominant effect of the jet on the flow field. Firstly, in Fig. 4(a) very good agreement can be observed between the profiles of the mean vertical velocity at the three Reynolds numbers in the case of $R_{SJ} = 0$. For $R_{SJ} = 0.5$, the distributions are also very similar and the discrepancies in the values do not exceed 4%. It clearly shows the deviation of the jet in the intermediate zone. Moreover, this shift

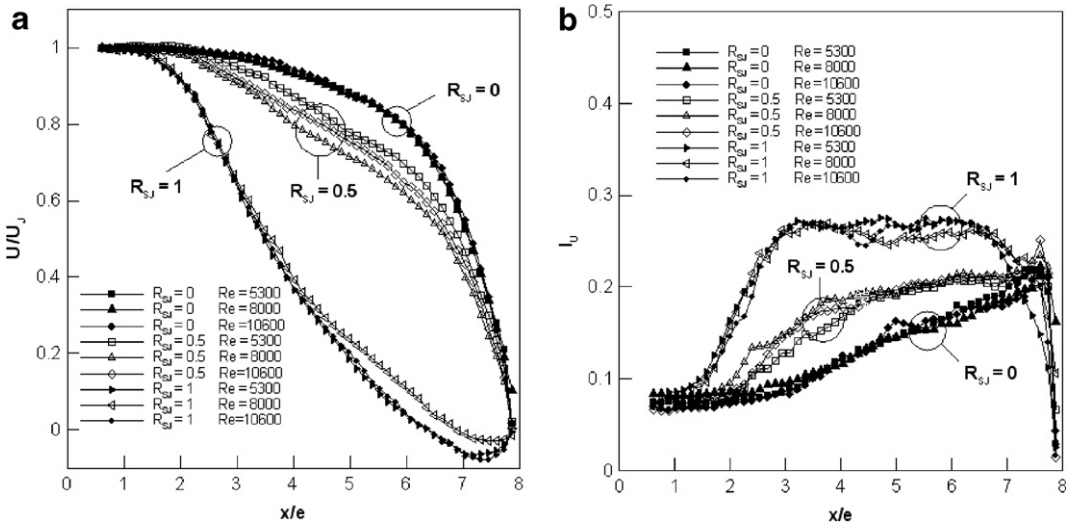


Fig. 4. Distributions along the jet centerline of the mean vertical velocity (a) and of the vertical turbulence intensity (b).

is initiated at the end of the potential core, which corresponds to a distance of 2.6$e$ in our case. For $R_{SJ} = 1$, the curves are likewise similar together showing a rapid decrease of the velocity that appears after only one nozzle width distance from the exit of the jet. These latter distributions of velocity thus demonstrate the strong deviation of the jet in this surface-to-jet velocity ratio. They also present negative values above $x/e = 6.5$, which is caused by the location of a recirculation region described later. The vertical turbulence intensity profiles illustrated in Fig. 4(b) also highlight the similarity of the measured values at the same surface-to-jet velocity ratio. The values of the $I_U$ turbulence intensity from $x/e = 1$ to 7 progressively rise with the increase in $R_{SJ}$ and reach a maximum of 27% in the cases of $R_{SJ} = 1$, which is caused by the location of a recirculation region. The development of this recirculation region will be discussed later.

Then, to compare the twelve cases, the time-averaged velocity magnitude and the two-component turbulent kinetic energy are depicted along the $y$-direction in the middle of the measurement area ($x/e = 4$) and near the impingement surface ($x/e = 7$) to describe the mean velocity field and the velocity fluctuation distribution, respectively (Fig. 5).

The velocity magnitude profiles at $x/e = 4$ and $x/e = 7$ are weakly affected by the surface-to-jet velocity ratios except in the case of $R_{SJ} = 1$. Nevertheless, a modification of the profiles for $y/e < 0$ and a slight shift of the maximum value locations to the right in the $y$-direction are observed when $R_{SJ}$ increases (Fig. 5(a)–(c)). In Fig. 5(d), a strong change of the velocity profiles is noticed at $x/e = 7$. It is important to emphasize the very good agreement between the same velocity profiles at the three Reynolds numbers. This good similarity can also be observed in the case of the two-component turbulent kinetic energy $k'$ profiles illustrated in Fig. 5(e)–(h). As previously, in the cases of $R_{SJ}$ up to 0.5, the $k'$ profiles are subjected to slight changes. The maximum peak values of the normalized $k'$ are about 0.06. In the case of $R_{SJ} = 1$ and at $x/e = 7$, the normalized $k'$ profiles present a high peak value of 0.012–0.016 located

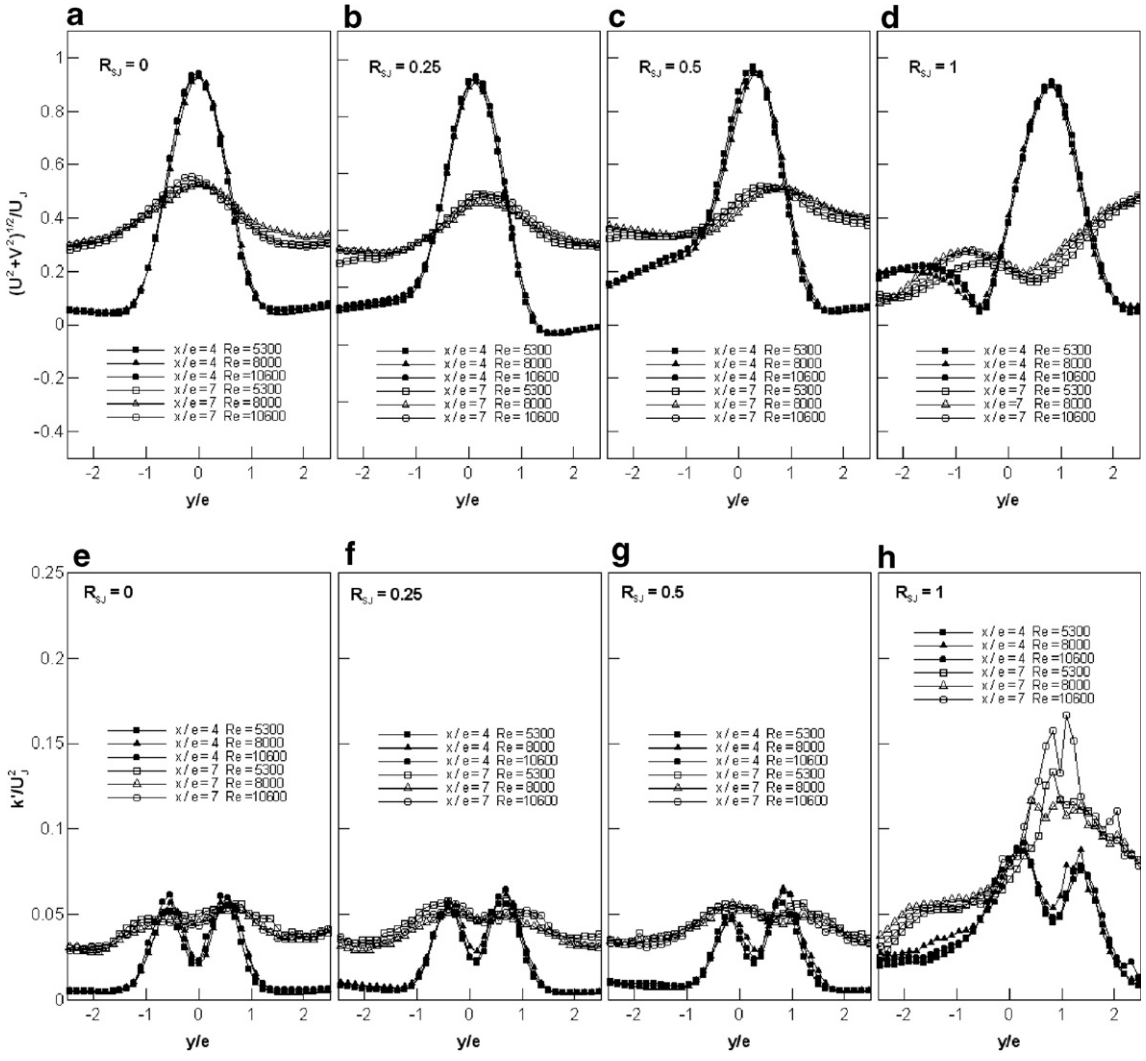


Fig. 5. Distributions in $y$-direction of the mean velocity magnitude: (a) $R_{SJ} = 0$, (b) $R_{SJ} = 0.25$, (c) $R_{SJ} = 0.5$, (d) $R_{SJ} = 1$ and of the two component turbulent kinetic energy: (e) $R_{SJ} = 0$, (f) $R_{SJ} = 0.25$, (g) $R_{SJ} = 0.5$, (h) $R_{SJ} = 1$.

at $y/e = 1$, which shows the high turbulent activity of this zone close to the stagnation point and located in the mixing region between the jet and a recirculation region described later.

The above considerations thus suggest that the surface-to-jet velocity ratio is the parameter influencing the flow field, the mean velocities and the turbulent quantities, independently of the Reynolds number in the studied range. This conclusion thereby justifies the next detailed analysis for only one Reynolds number ($Re = 10{,}600$). In addition, the work of Gradeck et al. (2005) on a circular water jet impinging on a moving surface can be mentioned. They cited the surface-to-jet velocity ratio as a main parameter influencing the radius of the hydraulic jump that appeared in their experiment. Finally, it is interesting to note that the surface-to-jet velocity ratio would be an additional parameter, and that of first importance, in the average Nusselt number correlation in comparison with that of jets impinging on a stationary surface (Martin, 1977).

### 3.2. Mean flow patterns

The time-averaged velocity magnitude and streamlines at $Re = 10{,}600$ for the surface-to-jet velocity ratios of 0, 0.25, 0.5 and 1 are represented in Fig. 6.

The first case (Fig. 6(a)) depicts a typical turbulent slot jet confined and submerged impinging on a stationary surface. Two recirculation patterns can be observed in the outflow (noted $A$ and $B$, respectively, for the left, upstream recirculation and right, downstream recirculation). The other characteristics of this flow field are the normal impingement of the jet, the symmetry of the velocity magnitude between the left and right wall jets and the stagnation point centered at $y/e = 0$. For quite the same configurations, the recirculation patterns were previously observed experimentally by Gupta (2005) at $Re = 7000$, by Beaubert (2002) in LES calculations at $Re = 3000$, 7500 and 13,500, and in DNS calculations by Abide (2005) at $Re = 3000$ or Hattori and Nagano (2004) at $Re = 4560$. They were also observed in the case of round confined and submerged turbulent impinging jets, experimentally by Fitzgerald and Garimella (1998), and numerically with the normal-velocity relaxation turbulence model ($v^2$–$f$ model) by Behnia et al. (1999).

The second case ($R_{SJ} = 0.25$) is presented in Fig. 6(b). The small surface-to-jet velocity ratio has a slight effect on the flow field. The jet is slightly deviated, thus the stagnation (or impingement) point moves to $y/e = 0.1$. The $B$ recirculation is not affected and the position of its center remains at $x/e = 5.6$. The most noticeable change is the displacement of the $A$ recirculation center from $x/e = 5.6$ to $x/e = 4.2$.

The third case ($R_{SJ} = 0.5$) can be seen in Fig. 6(c). The jet is a little more deviated, so that the stagnation point moves to $y/e = 0.4$. The center of the $A$ recirculation appears clearly on the field of view and is located at $x/e = 3.8$ and $y/e = -4.1$. The $B$ recirculation is slightly affected. The appearance of a detachment point at $y/e = -4.6$ can also be observed, induced by the expansion of a new recirculation region noted as $C$. This $C$

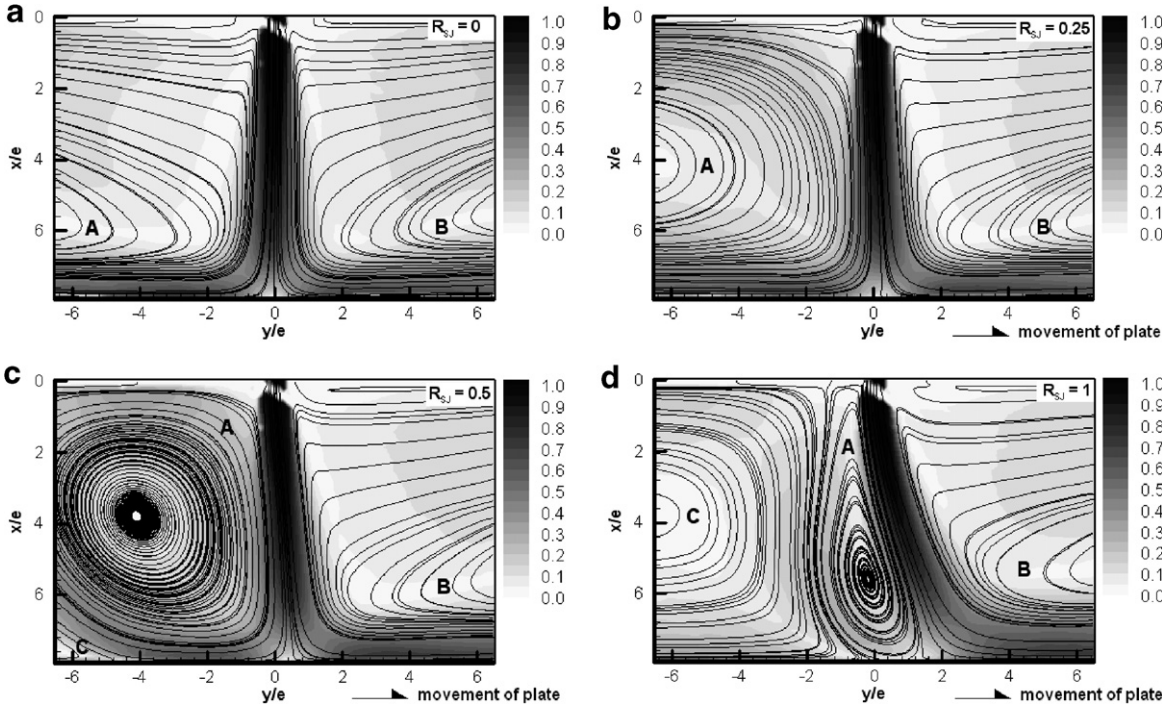


Fig. 6. Dimensionless mean velocity magnitude $(U^2 + V^2)^{1/2}/U_J$ and streamlines illustrating the recirculating flow patterns for $H/e = 8$, $Re = 10{,}600$: (a) $R_{SJ} = 0$, (b) $R_{SJ} = 0.25$, (c) $R_{SJ} = 0.5$, (d) $R_{SJ} = 1$.

recirculation is in the opposite direction relative to the $A$ recirculation. The decrease in the upstream wall jet velocity magnitude added to the other modifications leads to an asymmetry of the flow field patterns.

The last case ($R_{SJ} = 1$) depicted in Fig. 6(d) is the most affected case concerning the flow field. The jet is strongly deviated to the downstream part of the measurement area, which is corroborated by the movement of the impingement point to $y/e = 1.3$. The expansion of the $C$ recirculation compresses the $A$ recirculation and thus the $A$ recirculation center moves to $x/e = 5.6$ and $y/e = -0.2$, and the detachment point is shifted to $y/e = -0.4$. The left wall jet issuing from the jet is restrained between the detachment point and the stagnation point and is characterized by a low velocity magnitude. These observations confirm the previous calculations obtained from a $k$–$\varepsilon$ model used with the one-equation model of Wolfshtein in a similar case (Senter et al., 2005).

In Fig. 7, the distribution of the two-component turbulent kinetic energy is depicted. In the stationary case, the higher level zones of $k'/U_J^2$ correspond to the mixing layers of the wall jet, to the mixing layers of the jet and to the impinging zone. The peak values of the normalized quantity $k'$ reached in these regions are about 0.055, 0.066 and 0.069, respectively. In the case of $R_{SJ} = 0.25$, a slight increase in the peak value is noted in the impinging zone to 0.083. For $R_{SJ} = 0.5$, the peak value near the stagnation point also increases slightly and is about 0.086. The normalized $k'$ value close to the detachment point is about 0.059. Strong modifications of the distribution of $k'/U_J^2$ appear for $R_{SJ} = 1$. The high turbulent activity in the $A$ recirculation near the stagnation point is noteworthy. In this zone, the peak value of the normalized $k'$ reaches 0.166. Finally, the low values of the normalized $k'$ should be noted in the $C$ recirculation close to the impingement surface, about 0.017 at $y/e = -4$. Thus, it is clear that the $C$ recirculation in the case of $R_{SJ} = 1$ provides lower values of the normalized $k'$ in this region than the left wall jet flow for the previous surface-to-jet velocity ratios in the same region.

### 3.3. Mean velocity components

In Fig. 8 ($R_{SJ} = 0$), the mean and rms quantities of component $U$ are compared to the experimental values of Maurel (2001) and LES data of Beaubert (2002) for $H/e = 10$ and a Reynolds number of 13,500 to validate our experimental results. Fig. 8(a) shows good agreement of the time-averaged vertical velocity between these different data. The length of the potential core $L_C$ for experimental and numerical values at $H/e = 10$ and $Re = 13{,}500$ is about $0.37H$. In the case of $H/e = 8$ and $Re = 10{,}600$, $L_C$ is $0.32H$. This lower value can be explained by a lower nozzle-to-plate spacing, as mentioned by Maurel (2001), and also by a higher value of the turbulence intensity at the nozzle exit. Besides, Van and Howell (1976) stated that the length of the potential core linearly decreases with the increase in the initial turbulence intensity at the nozzle exit. Fig. 8(b) presents the centerline vertical turbulence intensity profiles. It appears that the profiles become very similar for $x/H > 0.4$. Thus, the turbulence intensity at the nozzle exit does not seem to influence the distribution of

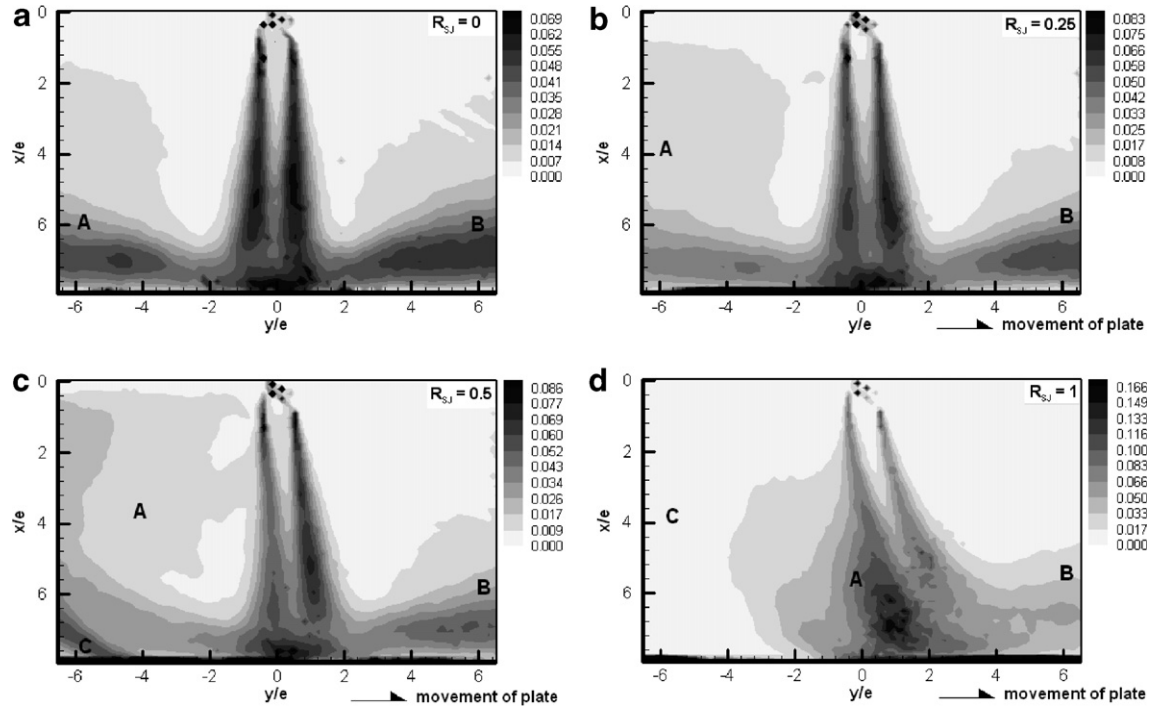


Fig. 7. Distribution of $k'/U_J^2$ for $H/e = 8$ and $Re = 10{,}600$: (a) $R_{SJ} = 0$, (b) $R_{SJ} = 0.25$, (c) $R_{SJ} = 0.5$, (d) $R_{SJ} = 1$.

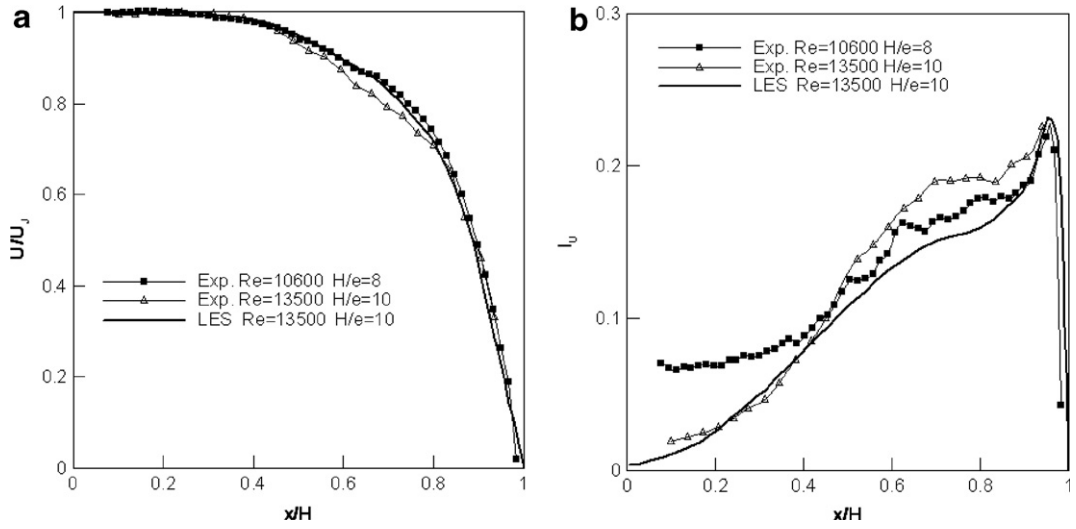


Fig. 8. Distributions along the jet centerline of the time-averaged vertical velocity (a) and of the vertical turbulence intensity (b).

the vertical turbulence intensity along the centerline in the intermediate zone nor in the impinging zone. In fact, the centerline turbulence intensity of component $U$ is close to 22% for the three cases at $x/H = 0.95$.

Next, the mean velocity components are discussed for the different surface-to-jet velocity ratios studied ($R_{SJ} = 0$, 0.25, 0.5 and 1) at $Re = 10{,}600$. They are also represented for the three flow regions of the impinging jet outlined in Fig. 9. Thus, Fig. 10(a)–(d) present the mean velocity of component $U$ along the $y$-direction for different $x$ locations, at $x/e = 1$ (in the potential core), $x/e = 4$ (in the intermediate zone) and $x/e = 7$ and 7.5 (in the impinging zone). The similarity of the profiles at the various $x$ locations for the surface-to-jet velocity ratios between 0 and 0.5 can be observed first. Indeed, in the potential core, the maximum value of the time-averaged velocity $U$ occurs at $y/e = 0$ and reaches $U_J$. Then, in the intermediate zone, the maximum value of $U$ reaches 0.95 $U_J$ at $y/e = 0$ for $R_{SJ} = 0$, at $y/e = 0.13$ for $R_{SJ} = 0.25$ and at $y/e = 0.29$ for $R_{SJ} = 0.5$. A slight deviation of the jet happens in the case of $R_{SJ} = 1$, since the maximum value of $U$ occurs at location $y/e = 0.83$ and its magnitude is reduced to 0.86 $U_J$. In the impinging zone, the same trend is noticed: for $R_{SJ} = 0$, 0.25 and 0.5, the jet is slightly deviated and the maxima of $U$ are quite similar and near to 0.52 $U_J$ at $x/e = 7$ and near to 0.33 $U_J$ at $x/e = 7.5$. For $R_{SJ} = 1$, the jet is significantly deviated and the maxima of $U$ decrease to 0.35 $U_J$ at $x/e = 7$ and to 0.20 $U_J$ at $x/e = 7.5$. The influence of the $A$ recirculation is observed from the different profiles at each $x$ location studied for the negative values of $y/e$. Fig. 10(e)–(h) show the normalized horizontal component of the velocity in the impinging zone for different $y$ locations ($y/e = -3$, $-1$, 0, 1, 3) respectively, for $R_{SJ} = 0$, 0.25, 0.5 and 1. For the stationary case, the symmetries between the profiles at $y/e = -3$ and 3 on the one hand, and at $y/e = -1$ and 1 on the other hand, confirm the symmetry of the left and right wall jets that normally occurred in this case. The almost null value of the time-averaged velocity $V$ on the centerline highlights the good accuracy of the experimental set-up and measurements. For $R_{SJ} = 0.25$, the trend of the velocity distribution does not change drastically. The slight deviation of the jet induces a slight increase in the absolute maximum value of $V$ at $y/e = -1$ and 0 and a slight decrease of the absolute maximum value of $V$ at $y/e = 1$. For $R_{SJ} = 0.5$, the asymmetry between the left and right wall jet is more pronounced. Thus, at $x/e = 7.73$, the normalized velocity of component $V$ is equal to $-0.62$ at $y/e = -3$ and 0.75 at $y/e = 3$, $-0.56$ at $y/e = -1$ and 0.25 at $y/e = 1$. For $R_{SJ} = 1$, the wall jets are completely asymmetrical. Indeed, the profiles of the velocity $V$ at the locations $y/e = -1$, 0 and 1 are affected by the $A$ recirculation, whereas at $y/e = -3$, the profile of the $V$ velocity is influenced by the $C$ recirculation and all the measurements at $x/e > 5$ become positive. Furthermore, the distribution of the $V$ velocity at $y/e = 3$ emphasizes the predominance of the right wall jet over the left one.

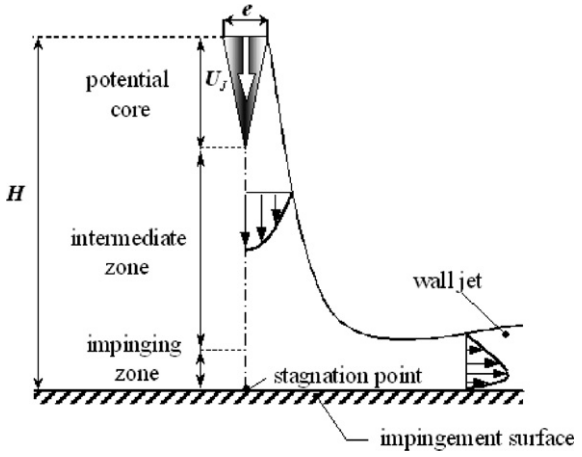


Fig. 9. Flow regions for an impinging jet.

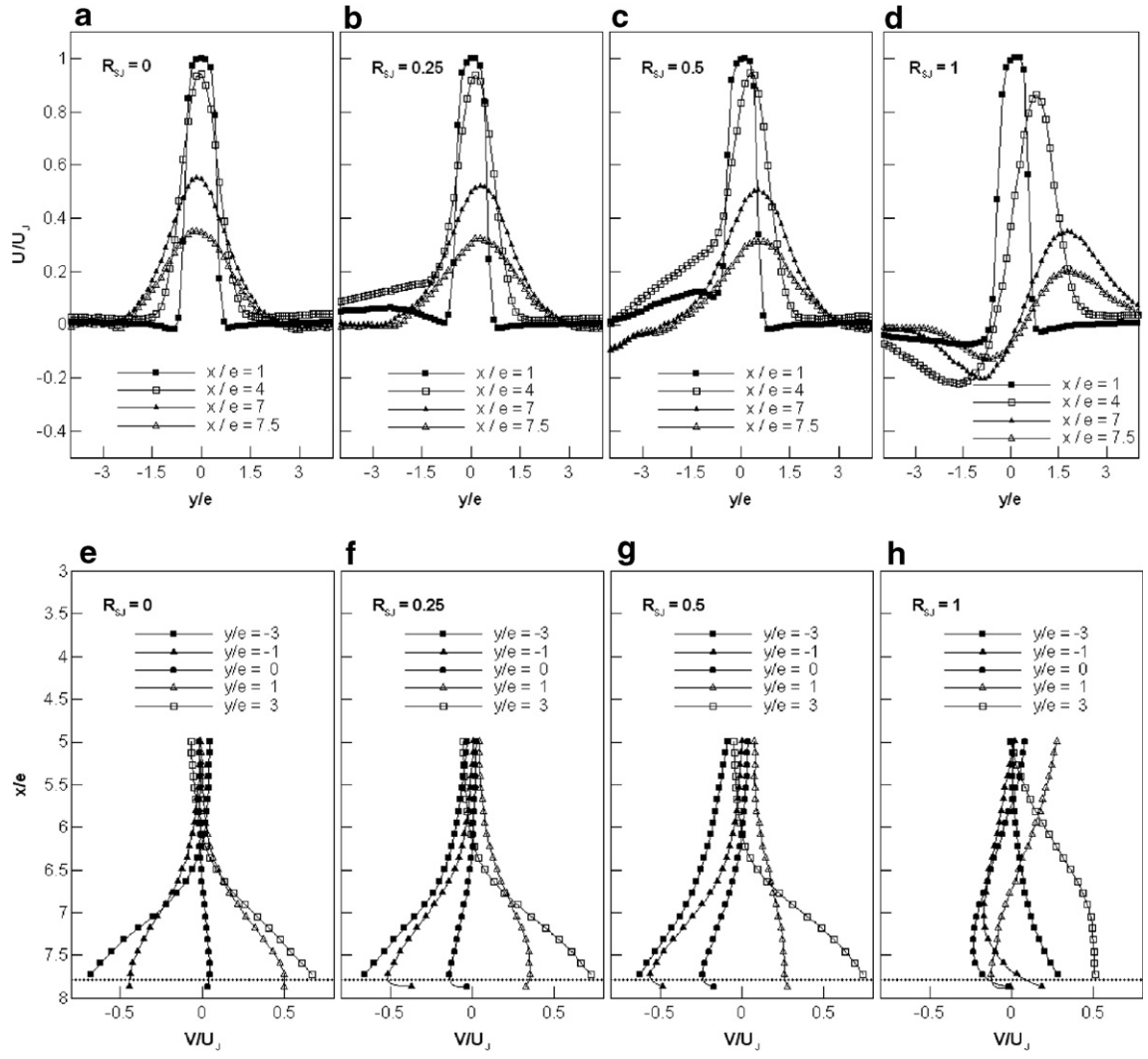


Fig. 10. Distributions of the mean vertical velocity along the $y$-direction: (a) $R_{SJ} = 0$, (b) $R_{SJ} = 0.25$, (c) $R_{SJ} = 0.5$, (d) $R_{SJ} = 1$ and of the mean horizontal velocity along the $x$-direction: (e) $R_{SJ} = 0$, (f) $R_{SJ} = 0.25$, (g) $R_{SJ} = 0.5$, (h) $R_{SJ} = 1$.

Consequently, the increase in the surface-to-jet velocity ratios progressively leads the wall jets to become strongly asymmetrical and thus to have an undeniably significant effect on the local convective heat transfer.

### 3.4. Reynolds stresses

The root of the normal stresses in the $x$- and $y$-directions, i.e. the turbulence intensities of components $U$ and $V$, and the Reynolds shear stress $\langle u'v' \rangle$ are illustrated in Fig. 11 for the different values of $R_{SJ}$ as a function of the non-dimensional distance $x/e$ for the five $y/e$ locations.

Fig. 11(a)–(d) depict the evolution of the $I_U$ turbulence intensity with the increase in the surface-to-jet velocity ratios. In the cases of $R_{SJ} = 0$ and 0.25, the distributions of $I_U$ are quite similar. For these two surface-to-jet velocity ratios, a peak value of $I_U$ appears in the neighbourhood of $x/e = 7.5$. At $y/e = -3$ and 3, these peaks are close to 13% and at $y/e = -1$, 0 and 1, they reach approximately 22%. A slight change is observed for $R_{SJ} = 0.5$, since the maximum of $I_U$ reaches 25% close to the stagnation point. The effect of the surface velocity on the $I_U$ distribution is more marked in the case of $R_{SJ} = 1$. At $y/e = -3$, the turbulence intensity $I_U$ is weaker than before and is less than 5% for $x/e > 7$. This is due to the influence of the $C$ recirculation at this $y$ location. At $y/e = -1$ and near the impingement surface, the turbulence intensity $I_U$ is also at a lower level than previously and is less than 10% over $x/e = 7$. At this position, the fluctuation of the $U$ velocity is influenced by the mixing layer between the $A$ and $C$ recirculations. At $y/e = 0$, the level of turbulence intensity increases up to 28%. This maximum occurs at $x/e = 5.5$ close to the center of the $A$ recirculation. The value of $I_U$ is even more significant at $y/e = 1$, in the mixing zone between the jet and the $A$ recirculation and close to the impingement. The peak value of $I_U$ is so within 33%. At $y/e = 3$, the profile of $I_U$ is very similar to the shape characterizing the previous distribution of $I_U$ in a wall jet, i.e. with a maximum intensity in the vicinity of $x/e = 7.5$. This peak value of $I_U$ is about 24%.

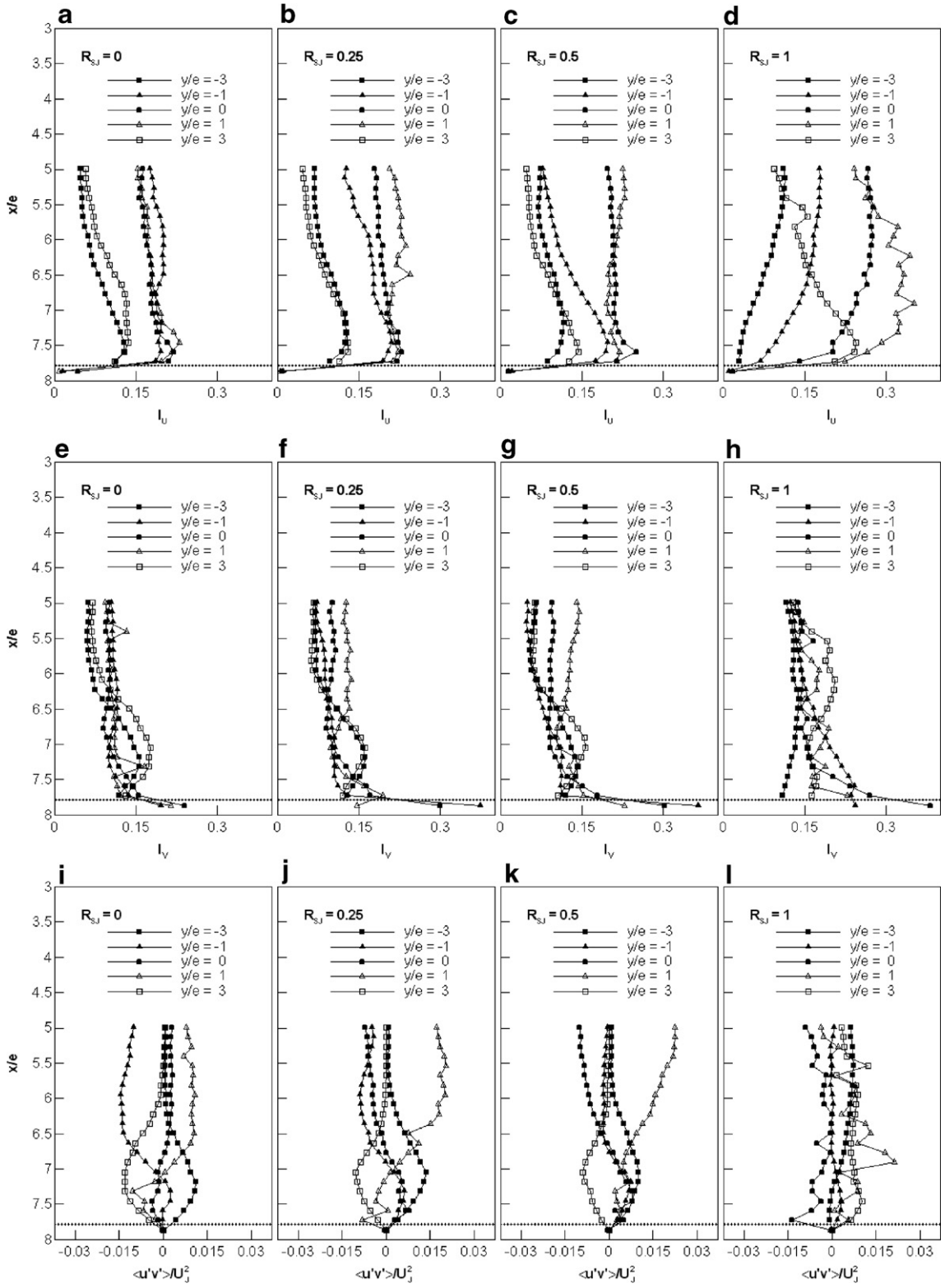


Fig. 11. Distribution of Reynolds stresses along the $x$-direction. $I_u$: (a) $R_{SJ} = 0$, (b) $R_{SJ} = 0.25$, (c) $R_{SJ} = 0.5$, (d) $R_{SJ} = 1$; $I_v$: (e) $R_{SJ} = 0$, (f) $R_{SJ} = 0.25$, (g) $R_{SJ} = 0.5$, (h) $R_{SJ} = 1$; $\langle u'v' \rangle / U_J^2$: (i) $R_{SJ} = 0$, (j) $R_{SJ} = 0.25$, (k) $R_{SJ} = 0.5$, (l) $R_{SJ} = 1$.

Fig. 11(e)–(h) report the $I_V$ turbulence intensity profiles. In the first three cases ($R_{SJ} = 0$, 0.25 and 0.5), the distributions of $I_V$ at the different $y$ locations do not significantly change for $x/e$ between 6.5 and 7.59. At $y/e = -1$, 0 and 1 and at these $x/e$, the values of $I_V$ are about 11%. The decrease of $I_V$ with the increase in $R_{SJ}$ at $y/e = -1$ in the zone $x/e < 6.5$ is explained by the progressive shift of the $A$ recirculation to the right. At $y/e = -3$ and 3, the

$I_V$ curves present a peak value of about 16% close to $x/e = 7$. As for previous observations, in the case of $R_{SJ} = 1$, the change in $I_V$ is more affected. We can pinpoint the peak value of 25% at $y/e = -1$, which shows an increase in $I_V$ in the mixing layer between the $A$ and the $C$ recirculations near the impingement surface. The high level of $I_V$ close to the detachment point is also noteworthy. The value of $I_V$ at $y/e = 0$ and $x/e = 7.73$ is, for instance, about 27%.

The Reynolds shear stress along the $x$-direction is depicted in Fig. 11(i)–(l) for each surface-to-jet velocity ratio. For $R_{SJ} = 0$, the Reynolds shear stress along the centerline is normally almost null. The distributions of $\langle u'v' \rangle$ at the locations $y/e = 1$ and $-1$, even at the Reynolds numbers of 5300 and 8000, highlight a characteristic point where the value of this quantity is systematically equal to zero at the same $x/e$ position of nearly 7.1. This singular phenomenon has previously been observed by Maurel and Solliec (2001). They noted that this point might characterize the transition of the intermediate zone to the beginning of the impinging one. Concerning the profiles at $y/e = 3$ and $-3$, they present an absolute peak value close to 0.012 at $x/e = 7.2$, which determines, respectively, the mixing layers between the $A$ recirculation and the upstream wall jet, and between the $B$ recirculation and the downstream wall jet. For $R_{SJ} = 0.25$, only the centerline distribution is affected and confirms the slight deviation of the jet to the right. For $R_{SJ} = 0.5$, all the values at $y/e = 1$ become positive. For $R_{SJ} = 1$, the marked changes of the flow field topology significantly influence the distribution of $\langle u'v' \rangle$. We can, for instance, notice the negative values of this quantity in the centerline, which corresponds to the location in the $A$ recirculation.

## 4. Conclusion

Particle image velocimetry measurements have been conducted to examine the flow field of a turbulent slot air jet confined and submerged impinging normally on a moving flat surface. It is developed in order to have a better understanding of the physical phenomenon. The surface-to-jet velocity ratio $R_{SJ}$ appears as the influencing parameter on the flow field topology, independently of the Reynolds number in the studied range. According to the mean velocities and turbulent quantities measured, the flow field is slightly affected for a surface-to-jet velocity ratio of 0.25. For this ratio, the flow field remains almost symmetric and the jet is slightly shifted to the downstream part of the tunnel. For a surface-to-jet velocity ratio of 0.5, the upstream main recirculation is significantly affected and a detachment point appears at a distance of 4.6 nozzle widths upstream from the centerline. A new recirculation thus emerges. The most affected topology occurs in the case of a surface-to-jet velocity ratio equal to unity. The jet is strongly deviated to the downstream part of the tunnel and the detachment point moves very close to the centerline. The previous emerging recirculation becomes prominent and the previous main recirculation is significantly reduced. Furthermore, the turbulence intensity measurements close to the stagnation region point out the increase in their value with the increase in the surface-to-jet velocity ratio. Finally, knowledge of the behaviour of the flow field provides crucial information for future numerical or experimental heat transfer studies in this case. Likewise upcoming studies will compare these experimental results with those obtained from RANS-based turbulence models, LES and DNS.

## References


Abide, S., 2005. A domain Decomposition Method Designed for Direct Numerical Simulation: Contribution to Plane Impinging Jets. Ph.D. thesis, University of Nantes, France.

Antonia, R.A., 1983. On the organized motion of a turbulent plane jet. J. Fluid Mech. 134, 49–66.

Awbi, H.B., 1991. Ventilation of Buildings. E&FN Spon.

Beaubert, F., 2002. Large Eddy Simulation of a Plane Turbulent Impinging Jet. Ph.D. thesis, University of Nantes, France.

Behnia, M., Parneix, S., Shabany, Y., Durbin, P.A., 1999. Numerical study of turbulent heat transfer in confined and unconfined impinging jets. Int. J. Heat Fluid Flow 20, 1–9.

Beitelmal, A.H., Saad, M.A., Patel, C.D., 2000. Effects of surface roughness on the average heat transfer of an impinging air jet. Int. Commun. Heat Mass Transfer 27 (1), 1–12.

Bruun, H.H., 1995. Hot-wire Anemometry, Principles and Signal Analysis. Oxford University Press, Oxford, pp. 405–445.

Chakroun, W.M., Abdel-Rahman, A.A., Al-Fahed, S.F., 1998. Appl. Therm. Eng. 18, 1225–1241.

Chattopadhyay, H., Saha, S.K., 2003. Turbulent flow and heat transfer from a slot jet impinging on a moving plate. Int. J. Heat Fluid Flow 24, 685–697.

Fitzgerald, J.A., Garimella, S.V., 1998. A study of the flow field of a confined and submerged impinging jet. Int. J. Heat Mass Transfer 41 (8-9), 1025–1034.

Gardon, R., Akfirat, J.C., 1965. The role of turbulence in determining the heat transfer characteristics of impinging jets. Int. J. Heat Mass Transfer 8, 1261–1272.

Gardon, R., Akfirat, J.C., 1966. Heat transfer characteristics of impinging two-dimensional air jets. ASME J. Heat Transfer 65, 101–108.

Gori, F., Bossi, L., 2003. Optimal slot height in the jet cooling of a circular cylinder. Appl. Therm. Eng. 23, 859–870.

Gradeck, M., Kouachi, A., Dani, A., Arnoult, D., Boréan, J.L., 2005. Experimental and numerical study of the hydraulic jump of an impinging jet on a moving surface. Exp. Therm. Fluid Sci. 30, 193–201.

Gupta, S., 2005. Experimental Analysis of the Dynamical Behaviour and Effectiveness of Air Curtains Designed for Cellular Confining. Ph.D. thesis, University of Nantes, France.

Haneda, Y., Tsuchiya, Y., Nakabe, K., Suzuki, K., 1998. Enhancement of impinging jet heat transfer by making use of mechano-fluid interactive flow oscillation. Int. J. Heat Fluid Flow 19, 115–124.

Hattori, H., Nagano, Y., 2004. Direct numerical simulation of turbulent heat transfer in plane impinging jet. Int. J. Heat Fluid Flow 25, 749–758.

Korger, M., Krizek, F., 1966. Mass-transfer coefficient in impingement flow from slotted nozzles. Int. J. Heat Mass Transfer 9, 337–344.

Martin, H., 1977. Heat and mass transfer between impinging gas jets and solid surfaces. Adv. Heat Transfer 13, 1–60.

Maurel, S., 2001. Experimental Study of the Impinging Plane Jet: Parametric Analysis and Characterisation of the Mass Transfers. Ph.D. thesis, University of Nantes, France.

Maurel, S., Solliec, C., 2001. A turbulent plane jet impinging nearby and far from a flat plate. Exp. Fluids 31, 687–696.

Metzger, D.E., 1962. Spot cooling and heating of surfaces with high velocity impinging air jets. Technical Report No. 52, Department of Mechanical Engineering, Stanford University.

Narayanan, V., Seyed-Yagoobi, J., Page, R.H., 2004. An experimental study of fluid mechanics and heat transfer in an impinging slot jet flow. Int. J. Heat Mass Transfer 47, 1827–1845.

Raffel, M., Willert, C., Kompenhans, J., 1998. Particle Image Velocimetry. Springer, Berlin.

Rajaratnam, N., 1976. Turbulent Jet. Elsevier Scientific Publishing Company, New York.

Sakakibara, J., Hishida, K., Maeda, M., 1997. Vortex structure and heat transfer in the stagnation region of an impinging plane jet (simultaneous measurements of velocity and temperature fields by digital particle image velocimetry and laser-induced fluorescence). Int. J. Heat Mass Transfer 40 (13), 3163–3176.

Schlünder, E.U., Krotzsch, P., Hennecke, Fr.-W., 1970. Gesetzmäßigkeiten der Wärme- und Stoffübertragung bei der Prallströmung aus Rund- und Schlitzdüsen. Chem.-Ing.-Tech. 42 (6), 333–428.

Senter, J., Solliec, C., Viazzo, S., 2005. Local convective heat transfer induced by a turbulent slot jet impinging on a moving flat surface. In: Eurotherm Seminar 77, Heat and Mass Transfer in Food Processing, Parma, Italy, June 20–22, 2005.

Subba Raju, K., Schlünder, E.U., 1977. Heat transfer between an impinging jet and a continuously moving surface. Wärme-Stoffübertrag. 10, 131–136.

Van, N.Q., Howell, R.H., 1976. Influence of the initial turbulence intensity on the development of plane air-curtain jets. ASHRAE Trans., 2396.

Van Heiningen, A.R.P., Mujumdar, A.S., Douglas, W.J.M., 1977. Flow and heat transfer characteristics of a turbulent slot jet impinging on a moving wall. In: Abstracts of the Symposium on Turbulent Shear Flows, Pennsylvania State University, University Park, PA 1, pp. 3.9–3.15.

Viskanta, R., 1993. Heat transfer to impinging isothermal gas and flame jets. Exp. Therm. Fluid Sci. 6, 111–134.

Zumbrunnen, D.A., 1991. Convective heat and mass transfer in the stagnation region of a laminar planar jet impinging on a moving surface. ASME J. Heat Transfer 113, 563–570.